Soft Matter

Accepted Manuscript

ROYAL SOCIETY OF CHEMISTRY

www.rsc.org/softmatter

ARTICLE TYPE
www. rsc.org/xxxxxx | XXXXXXXX

Saddle-splay screening and chiral symmetry breaking in toroidal nematics

Vinzenz Koning,[*a] **Benjamin C. van Zuiden,**[a] **Randall D. Kamien**[b] **and Vincenzo Vitelli**[a]

Received Xth XXXXXXXXXX 20XX, Accepted Xth XXXXXXXXX 20XX
First published on the web Xth XXXXXXXXXX 200X
DOI: 10.1039/b000000x

We present a theoretical study of director fields in toroidal geometries with degenerate planar boundary conditions. We find spontaneous chirality: despite the achiral nature of nematics the director configuration shows a handedness if the toroid is thick enough. In the chiral state the director field displays a double twist, whereas in the achiral state there is only bend deformation. The critical thickness increases as the difference between the twist and saddle-splay moduli grows. A positive saddle-splay modulus prefers alignment along the short circle of the bounding torus, and hence promotes a chiral configuration. The chiral-achiral transition mimics the order-disorder transition of the mean-field Ising model. The role of the magnetisation in the Ising model is played by the degree of twist. The role of the temperature is played by the aspect ratio of the torus. Remarkably, an external field does not break the chiral symmetry explicitly, but shifts the transition. In the case of toroidal cholesterics, we do find a preference for one chirality over the other – the molecular chirality acts as a field in the Ising analogy.

1 Introduction

The confinement of liquid crystals in non-trivial geometries forms a rich and interesting area of study because the preferred alignment at the *curved* bounding surface induces bulk distortions of the liquid crystal – that is, the boundary conditions *matter*. This results in a great diversity of assemblies and mechanical phenomena[1–5]. Water droplets dispersed in a nematic liquid crystal interact and assemble into chains due to the presence of the anisotropic host fluid[6–8], defect lines in cholesteric liquid crystals can be knotted and linked around colloidal particles[9–12], and surface defects in spherical nematic shells can abruptly migrate when the thickness inhomogeneity of the shell is altered[13,14]. In the examples above spherical droplets (or colloids), either filled with – or dispersed in – a liquid crystal, create architectures arising from their coupling to the orientational order of the liquid crystal. Nematic structures where the bounding surface of the colloid or the liquid crystal droplet is topologically different from a sphere have also been studied[15–17]. Though there has been much interest in the interplay between order and toroidal geometries[17–25], it was only recently that experimental realisations of nematic liquid crystal droplets with toroidal boundaries were reported[26,27]. Polarised microscopy revealed a twisted nematic orientation in droplets with planar degenerate (tangential) boundary conditions, despite the achiral nature of nematics. This phenomenon, which we will identify as spontaneous chiral symmetry breaking [*], is subject of theoretical study in this article. The chirality of nematic toroids is displayed by the the local average orientation of the nematic molecules, called the director field and indicated by the unit vector $\mathbf{n}$. Motivated by experiment, we will assume this director field to be aligned in the tangent plane of the bounding torus. Fig. 1a shows an achiral nematic toroid which has its fieldlines aligned along the azimuthal direction, $\hat{\phi}$. In contrast, the chiral nematic toroids in Figs. 1b and 1c show a right and left handedness, respectively, when following the fieldlines anticlockwise (in the azimuthal direction). The

Fig. 1 Schematic of (a) achiral, (b) righthanded and (c) lefthanded toroidal nematic liquid crystals. The black lines are director field lines on the bounding torus.

origin of the chirality lies in two elastic effects of geometric confinement. Firstly, there is a trade-off between bend and twist deformations. Secondly, another type of director distortion called saddle-splay couples the director to the curvature of the boundary, and can consequently favour the chiral state.

These nematic toroids share similarites with polymer bundles[20,28–33]. In fact, twisted DNA toroids have been analysed

[a] *Instituut-Lorentz, Universiteit Leiden, Postbus 9506, 2300 RA Leiden, The Netherlands. * E-mail: koning@lorentz.leidenuniv.nl*
[b] *Department of Physics and Astronomy, University of Pennsylvania, Philadelphia, Pennsylvania 19104, USA.*

[*] Technically, it is spontaneous *achiral* symmetry breaking since the symmetry is the *lack* of chirality. However, we will conform to the standard convention.

with liquid crystal theory[20,32,34]. Under the appropriate solvent conditions DNA condenses into toroids[28,35]. These efficient packings of genetic material are interesting as vehicles in therapeutic gene delivery; it has been argued[20] that a twist in DNA toroids, for which there are indications both in simulations[36,37] and experiments[38], would unfold more slowly and could therefore be beneficial for this delivery process. Thus, besides a way to engineer complex structures, the theory of geometrically confined liquid crystals may also provide understanding of biological systems.

The organisation of this article is as follows. In section 2 we will discuss our calculational method which involves a single variational Ansatz only for the director fields of both chiral and achiral toroidal nematics. In section 3 we will consider its energetics in relation to the slenderness, elastic anisotropies, cholesteric pitch and external fields, and discuss the achiral-chiral transition in the light of the mean field treatment of the Ising model. Finally, we conclude in section 4.

2 Toroidal director fields

2.1 Free energy of a nematic toroid

We will study the general case in which the director lies in the tangent plane of the boundary assuming that the anchoring is strong so that the only energy arises from elastic deformations captured by the Frank free energy functional[39,40]:

$$\begin{aligned} F[\mathbf{n}(\mathbf{x})] = \frac{1}{2}\int \mathrm{d}V \Big(& K_1 (\nabla\cdot\mathbf{n})^2 \\ & + K_2 (\mathbf{n}\cdot\nabla\times\mathbf{n})^2 + K_3 (\mathbf{n}\times\nabla\times\mathbf{n})^2 \Big) \\ & - K_{24}\int \mathbf{dS}\cdot(\mathbf{n}\nabla\cdot\mathbf{n} + \mathbf{n}\times\nabla\times\mathbf{n}), \end{aligned} \tag{1}$$

where $\mathrm{d}\mathbf{S} = \boldsymbol{\nu}\,\mathrm{d}S$ is the area element, with $\boldsymbol{\nu}$ the unit normal vector (outward pointing) and where $\mathrm{d}V$ is the volume element. Due to the anisotropic nature of the nematic liquid crystal, this expression contains three bulk elastic moduli, K_1, K_2, K_3, rather than a single one for fully rotationally symmetric systems. In addition, there is a surface elastic constant K_{24}. K_1, K_2, K_3 and K_{24} measure the magnitude of splay, twist, bend and saddle-splay distortions, respectively. We now provide a geometrical interpretation of the saddle-splay distortions. Firstly, observe that under perfect planar anchoring conditions $\mathbf{n}\cdot\boldsymbol{\nu} = 0$ and so the first term in the saddle-splay energy does not contribute:

$$F_{24} = -K_{24}\int \mathrm{d}S\, \boldsymbol{\nu}\cdot(\mathbf{n}\times\nabla\times\mathbf{n}). \tag{2}$$

This remaining term in the saddle-splay energy is often rewritten as

$$F_{24} = K_{24}\int \mathrm{d}S\, \boldsymbol{\nu}\cdot(\mathbf{n}\cdot\nabla)\,\mathbf{n}. \tag{3}$$

because

$$\begin{aligned} (\mathbf{n}\times\nabla\times\mathbf{n})_a &= \epsilon_{abc} n_b \epsilon_{cpq}\partial_p n_q & (4)\\ &= (\delta_{ap}\delta_{bq} - \delta_{aq}\delta_{bp})\, n_b \partial_p n_q \\ &= -n_b\partial_b n_a & (5) \end{aligned}$$

where in the last line one uses that $0 = \partial_a(1) = \partial_a(n_b n_b) = 2n_b\partial_a n_b$. In other words, the bend is precisely the curvature of the integral curves of $\mathbf{n}$. Employing the product rule of differention $0 = \partial_a(\nu_b n_b) = \nu_b\partial_a n_b + n_b\partial_a\nu_b$ yields

$$F_{24} = -K_{24}\int \mathrm{d}S\, \mathbf{n}\cdot(\mathbf{n}\cdot\nabla)\,\boldsymbol{\nu}. \tag{6}$$

Upon writing $\mathbf{n} = n_1\boldsymbol{e}_1 + n_2\boldsymbol{e}_2$, with $\boldsymbol{e}_1$ and $\boldsymbol{e}_1$ two orthonormal basis vectors in the plane of the surface, one obtains

$$F_{24} = K_{24}\int \mathrm{d}S\, n_i L_{ij} n_j, \tag{7}$$

where we note that $i, j = 1, 2$ (rather than running till 3). Thus the nematic director couples to the extrinsic curvature tensor[41], defined as

$$L_{ij} = -\boldsymbol{e}_i\cdot(\boldsymbol{e}_j\cdot\nabla)\,\boldsymbol{\nu}. \tag{8}$$

If $\boldsymbol{e}_1$ and $\boldsymbol{e}_2$ are in the directions of principal curvatures, κ_1 and κ_2, respectively, one finds

$$F_{24} = K_{24}\int dS\,(\kappa_1 n_1^2 + \kappa_2 n_2^2). \tag{9}$$

We conclude that the saddle-splay term favours alignment of the director along the direction with the smallest principal curvature if $K_{24} > 0$. The controversial surface energy density $K_{13}\mathbf{n}\nabla\cdot\mathbf{n}$ is sometimes incorporated in eq. (1), but is in our case irrelevant, because the normal vector is perpendicular to $\mathbf{n}$, and so $\mathbf{n}\cdot\boldsymbol{\nu} = 0$.

We will consider a nematic liquid crystal confined in a handle body bounded by a torus given by the following implicit equation for the cartesian coordinates x, y, and z:

$$\left(R_1 - \sqrt{x^2+y^2}\right)^2 + z^2 \le R_2^2. \tag{10}$$

Here, R_1 and R_2 are the large and small radii, respectively, of the circles that characterise the outer surface: a torus obtained by revolving a circle of radius R_2 around the z-axis (Fig. 2). We can conveniently parametrise this solid torus by the coordinates $r \in [0, R_2]$, $\phi \in [0, 2\pi)$ and $\psi \in [0, 2\pi)$ (illustrated in Fig. 2):

$$x = (R_1 + r\cos\psi)\cos\phi, \tag{11}$$
$$y = (R_1 + r\cos\psi)\sin\phi, \tag{12}$$
$$z = r\sin\psi. \tag{13}$$

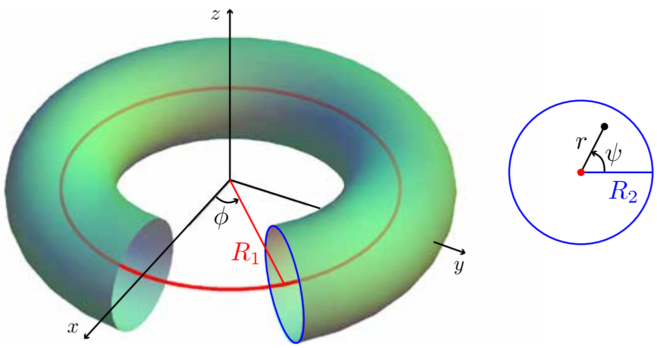

Fig. 2 *Left panel*: Schematic of the boundary of the geometry specified eq. (10) including graphical definitions of ϕ and R_1. The torus characterised by a large (red) and a small (blue) circle. The large circle, or centerline, has radius R_1. *Right panel*: Schematic of a cut including graphical definitions of r, ψ and R_2.

The metric reads:

$$g_{\mu\nu} = \begin{pmatrix} 1 & 0 & 0 \\ 0 & (R_1 + r\cos\psi)^2 & 0 \\ 0 & 0 & r^2 \end{pmatrix}, \qquad (14)$$

with $\mu, \nu \in \{r, \phi, \psi\}$. It follows that $\mathrm{d}\mathbf{S} = \boldsymbol{\nu}\sqrt{g}\,\mathrm{d}\psi\,\mathrm{d}\phi$ and $\mathrm{d}V = \sqrt{g}\,\mathrm{d}r\,\mathrm{d}\psi\,\mathrm{d}\phi$, where $g = \det g_{\mu\nu}$.

For a torus the ϕ and ψ directions are the principal directions. The curvature along the ψ direction is everywhere negative (measured with respect to the outward pointing normal) and the smallest of the two, so when $K_{24} > 0$, the director tends to wind along the small circle with radius R_2.

2.2 Double twist

To minimise the Frank energy we formulate a variational Ansatz built on several simplifying assumptions [20]. We consider a director field which has no radial component (*i.e.* $n_r = 0$), is tangential to the centerline ($r = 0$), and is independent of ϕ. Furthermore, since we expect the splay (K_1) distortions to be unimportant, we first take the field to be divergence free (*i.e.* $\nabla \cdot \mathbf{n} = 0$). Recalling that in curvilinear coordinates the divergence is $\nabla \cdot \mathbf{n} = \frac{1}{\sqrt{g}}\partial_\mu\left(\sqrt{g}n^\mu\right)$, we write :

$$n_\psi = \frac{f(r)\,R_1}{\sqrt{g_{\phi\phi}}} \qquad (15)$$

where the other terms in $\sqrt{g}$ play no role as they are independent of ψ. The ϕ-component of the director follows from the normalisation condition. For the radial dependence of $f(r)$ we make the simplest choice:

$$f(r) = \frac{\omega r}{R_2} \qquad (16)$$

and obtain

$$n_\psi = \omega\frac{\xi r/R_2}{\xi + \frac{r}{R_2}\cos\psi}, \qquad (17)$$

where we have introduced $\xi \equiv R_1/R_2$, the slenderness or aspect ratio of the torus. The variational parameter ω governs the chirality of the toroidal director field. If $\omega = 0$ the director field corresponds to the axial configuration (Fig 1a). The sign of ω determines the chirality: right handed when $\omega > 0$ (Fig. 1c) and left handed when $\omega < 0$ (Fig. 1b). The magnitude of ω determines the degree of twist. Note that the direction of twist is in the radial direction, as illustrated in Fig. 3. Therefore the

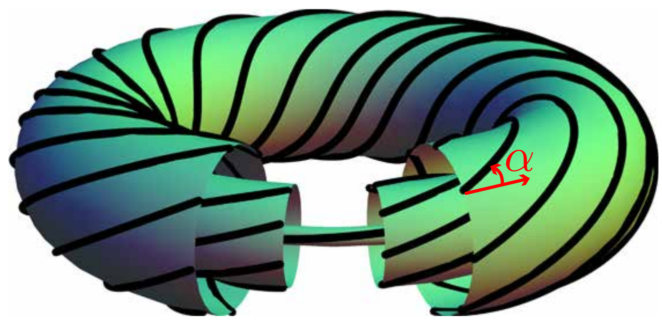

Fig. 3 Schematic of the Ansatz for the director fieldlines ($\omega = 0.6$ and $\xi = 3$), displaying a twist when going radially outward, including a graphical definition of α.

toroidal nematic is doubly twisted, resembling the cylindrical building blocks of the blue phases [39,40]. It may be useful to relate ω with a quantity at the surface, say the angle, α, that the director makes with $\hat{\phi}$. For the Ansatz, this angle will be different depending on whether one measures at the inner or outer part of the torus, but for large ξ we find

$$\omega \approx n_\psi\Big|_{r=R_2} = \sin\alpha. \qquad (18)$$

3 Chiral symmetry breaking

3.1 Results for divergence-free field

Since ω only determines the chirality of the double-twisted configuration but not the amount of twist, the free energy is invariant under reversal of the sign of ω, *i.e.* $F(-\omega) = F(\omega)$. This mirror symmetry allows us to write down a Landau-like expansion in which F only contains even powers of ω,

$$F = a_0(\{K_i\},\xi) + a_2(\{K_i\},\xi)\,\omega^2 + a_4(\{K_i\},\xi)\,\omega^4 + \mathcal{O}\left(\omega^6\right) \qquad (19)$$

where $\{K_i\}$ is the set of elastic constants †. If the coefficient $a_2 > 0$, the achiral nematic toroid ($\omega_{eq} = 0$) corresponds to

† Explicitly: $\{K_i\} = \{K_1, K_2, K_3, K_{24}\}$

the minimum of F provided that $a_4 > 0$. In contrast, the mirror symmetry is broken spontaneously whenever $a_2 < 0$ (and $a_4 > 0$). The achiral-chiral critical transition at $a_2 = 0$ belongs to the universality class of the mean-field Ising model. Therefore, we can immediately infer that the value of the critical exponent β in $\omega_{eq} \sim (-a_2)^\beta$ is $\frac{1}{2}$. To obtain the dependence of the coefficients a_i on the elastic constants and ξ, we need to evaluate the integral in eq. (1). We find for the bend, twist and saddle-splay energies:

$$\frac{F_3}{K_3 R_1} = 2\pi^2 \left(\xi - \sqrt{\xi^2 - 1}\right)/\xi + \pi^2 \frac{\xi\left(1 - 9\xi^2 + 6\xi^4 + 6\xi\sqrt{\xi^2-1} - 6\xi^3\sqrt{\xi^2-1}\right)}{\left(\xi^2-1\right)^{\frac{3}{2}}}\omega^2 + \mathcal{O}\left(\omega^4\right), \tag{20}$$

$$\frac{F_2}{K_2 R_1} = 4\pi^2 \frac{\xi^3}{\left(\xi^2-1\right)^{\frac{3}{2}}}\omega^2 + \mathcal{O}\left(\omega^6\right), \tag{21}$$

$$\frac{F_{24}}{K_{24} R_1} = -4\pi^2 \frac{\xi^3}{\left(\xi^2-1\right)^{\frac{3}{2}}}\omega^2. \tag{22}$$

Though the bend and twist energies are Taylor expansions in ω, the saddle-splay energy is exact. The large ξ asymptotic behavior of the elastic energy reads‡:

$$\frac{F}{K_3 R_1} \approx \frac{\pi^2}{\xi^2} + 4\pi^2\left(k - \frac{5}{16\xi^2}\right)\omega^2 + \frac{\pi^2}{2}\omega^4 + \mathcal{O}\left(\omega^6\right), \tag{23}$$

where $k \equiv \frac{K_2 - K_{24}}{K_3}$ is the elastic anisotropy in twist and saddle-splay. The achiral configuration contains only bend energy. For sufficiently thick toroids, bend distortions are exchanged with twist and the mirror symmetry is indeed broken spontaneously (Fig. 4). Interestingly, if $K_{24} > 0$ the saddle-splay deformations screen the cost of twist. If $K_{24} < 0$ on the other hand, there is an extra penalty for twisting. Setting the coefficient of the ω^2 term equal to zero yields the phase boundary:

$$k_c = \frac{-1 + 9\xi_c^2 - 6\xi_c^4 - 6\xi_c\sqrt{\xi_c^2-1} + 6\xi_c^3\sqrt{\xi_c^2-1}}{4\xi_c^2} \approx \frac{5}{16\xi_c^2} \qquad \text{if } \xi \gg 1 \tag{24}$$

Fig.5 shows the phase diagram as a function of ξ and k. It is interesting to look at the critical behavior. The degree of twist close to the transition is

$$\alpha_{eq} \approx \omega_{eq} \approx 2\left(\frac{5}{16\xi^2} - k\right)^{1/2} \tag{25}$$

‡ The fourth order term in the bend energy for general ξ, that reduces to $\frac{\pi^2}{2}K_3 R_2 \xi \omega^4$ in eq. 23, is not given in eq. (20), because it is too lengthy.

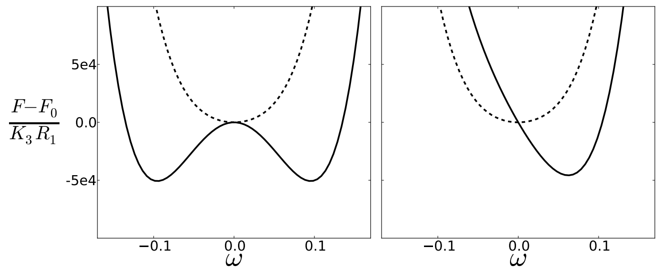

Fig. 4 *Left panel:* The free energy as a function of ω for $\xi = 6$ (dashed) and $\xi = 5$ (solid), when $(K_2 - K_{24})/K_3 = 10^{-2}$. For $\xi = 5$ the chiral symmetry is broken spontaneously: the minimum values of the energy occurs for a nonzero ω. *Right panel:* The free energy as a function of ω for $q = 0$ (dashed) and $qR_2 = 10^{-3}$ (solid), when $\xi = 6$, $(K_2 - K_{24})/K_3 = 10^{-2}$ and $K_2/K_3 = 0.3$. For $qR_2 = 10^{-3}$ the chiral symmetry is broken explicitly: the minimum value of the energy occurs for a nonzero ω, because F contains term linear in ω.

where we have used that $\sin\alpha_{eq} \approx \alpha_{eq}$ for small α_{eq}. Upon expanding $\xi = \xi_c + \delta\xi$ (with $\delta\xi < 0$) and $k = k_c + \delta k$ (with $\delta k < 0$) around their critical values ξ_c and k_c, respectively, we obtain the following scaling relations:

$$\alpha_{eq} \approx \frac{\sqrt{5}}{2}\left(-\frac{\delta\xi}{\xi_c^3}\right)^{1/2} \tag{26}$$

$$\alpha_{eq} \approx 2\left(-\delta k\right)^{1/2} \tag{27}$$

while keeping k and ξ fixed, respectively. Eqs. 26 and 27 are analogues to $m_{eq} \sim (-t)^{1/2}$, relating the equilibrium magnetisation, m_{eq} (in the ferromagnetic phase of the Ising model in Landau theory), to the reduced temperature, t.

3.2 Effects of external fields and cholesteric pitch

Due to the inversion symmetry of nematics, $F[\mathbf{n}] = F[-\mathbf{n}]$, an external magnetic field, $\mathbf{H}$, couples quadratically to the components of $\mathbf{n}$ rather than linearly as in spin systems. The magnetic free energy contribution reads:

$$F_m = -\frac{\chi_a}{2}\int \mathrm{d}V\left(\mathbf{n}\cdot\mathbf{H}\right)^2, \tag{28}$$

where $\chi_a = \chi_\parallel - \chi_\perp$, the difference between the magnetic susceptibilities parallel and perpendicular to $\mathbf{n}$. Consequently, there is no explicit chiral symmetry breaking due to $\mathbf{H}$ as is the case in the Ising model. Rather, $\mathbf{H}$ shifts the location of the critical transition in the phase diagram. For concreteness, we will consider two different applied fields, namely a uniaxial field $\mathbf{H} = H_z\hat{\mathbf{z}} = H_z\sin(\psi)\hat{\mathbf{r}} + H_z\cos(\psi)\hat{\boldsymbol{\psi}}$ and an azimuthal field $\mathbf{H} = H_\phi\hat{\boldsymbol{\phi}}$, as if produced by a conducting wire going

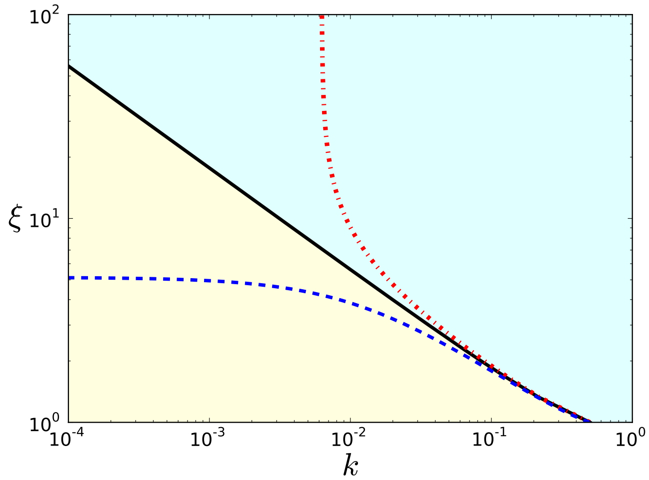

Fig. 5 Phase diagram as a function of the toroidal slenderness and the elastic anisotropy in twist and saddle-splay constant, $k \equiv (K_2 - K_{24})/K_3$. The twisted (yellow region) and axial (cyan region) configuration are separated by a boundary line in the absence of an external field (solid black), when $\mathbf{H} = \sqrt{0.1K_3}/\left(\sqrt{\chi_a}R_2\right)\hat{\boldsymbol{\phi}}$ (dashed blue) and when $\mathbf{H} = \sqrt{0.1K_3}/\left(\sqrt{\chi_a}R_2\right)\hat{\mathbf{z}}$ (dash-dotted red).

through the hole of the toroid. For $\mathbf{H} = H_z\hat{\mathbf{z}}$ we find

$$\begin{aligned} F_m &= -\pi^2\chi_a H_z^2 R_1 R_2^2 \xi^2 \left(2\xi\left(\xi - \sqrt{\xi^2-1}\right) - 1\right)\omega^2 \\ &\approx -\frac{\pi^2}{4}\chi_a H_z^2 R_1 R_2^2 \omega^2 \qquad \text{if } \xi \gg 1. \end{aligned} \tag{29}$$

For a positive χ_a this energy contribution is negative, implying that a larger area in the phase diagram is occupied by the twisted configuration. The new phase boundary (Fig. 5), which is now a surface in the volume spanned by ξ, k and H_z instead of a line, reads:

$$\begin{aligned} k_c = &\Big[-1 + 9\xi_c^2 - 6\xi_c^4 - 6\xi_c\sqrt{\xi_c^2-1} + 6\xi_c^3\sqrt{\xi_c^2-1} \\ &- \frac{\chi_a (H_z)_c^2 R_2^2}{K_3}\left(\xi_c^2 - 1\right)\xi_c \\ &\times\left(-2\xi_c + 2\xi_c^3 + \sqrt{\xi_c^2-1} - 2\xi_c^2\sqrt{\xi_c^2-1}\right)\Big] / \left(4\xi_c^2\right) \\ \approx &\frac{5}{16\xi_c^2} + \frac{\chi_a (H_z)_c^2 R_2^2}{16K_3} \qquad \text{if } \xi \gg 1. \end{aligned} \tag{30}$$

In contrast, an azimuthal field favours the axial configuration, contributing a postive ω^2-term to the energy when $\chi_a > 0$:

$$\begin{aligned} F_m &= -\pi^2\chi_a H_\phi^2 R_1 R_2^2 \\ &+ \frac{2\pi^2}{3}\chi_a H_\phi^2 R_1 R_2^2 \xi\left(2\xi^2\left(\xi - \sqrt{\xi^2-1}\right) - \sqrt{\xi^2-1}\right)\omega^2 \\ &\approx -\pi^2\chi_a H_\phi^2 R_1 R_2^2 + \frac{\pi^2}{2}\chi_a H_\phi^2 R_1 R_2^2\omega^2 \quad \text{if } \xi \gg 1. \end{aligned} \tag{31}$$

Consequently, this yields a shifted phase boundary (Fig. 5):

$$\begin{aligned} k_c = &\Big[-1 + 9\xi_c^2 - 6\xi_c^4 - 6\xi_c\sqrt{\xi_c^2-1} + 6\xi_c^3\sqrt{\xi_c^2-1} \\ &- \frac{2\chi_a (H_\phi)_c^2 R_2^2}{3K_3}\left(\xi_c^2 - 1\right) \\ &\times\left(1 + \xi_c^2 - 2\xi_c^4 + 2\xi_c^3\sqrt{\xi_c^2-1}\right)\Big] / \left(4\xi_c^2\right) \\ \approx &\frac{5}{16\xi_c^2} - \frac{\chi_a (H_\phi)_c^2 R_2^2}{8K_3} \qquad \text{if } \xi \gg 1. \end{aligned} \tag{32}$$

Similar results (eqs. (29) to (32)) hold for an applied electric field $\mathbf{E}$ instead of a magnetic field; the analog of χ_a is the dielectric anisotropy. There could however be another physical mechanism at play in a nematic insulator, namely the flexoelectric effect[39,42]. Splay and bend deformations induce a polarisation

$$\mathbf{P} = e_1\mathbf{n}\nabla\cdot\mathbf{n} + e_3\mathbf{n}\times\nabla\times\mathbf{n}, \tag{33}$$

where e_1 and e_3 are called the flexoelectric coefficients. Note that the first term in eq. 33 is irrelevant for the divergence-free Ansatz. A coupling of $\mathbf{P}$ with $\mathbf{E}$

$$F_P = -\int dV\,\mathbf{P}\cdot\mathbf{E} \tag{34}$$

could potentially lead to a shift of the transition. In the particuar case when $\mathbf{E} = E_z\hat{\mathbf{z}} = E_z\sin(\psi)\hat{\mathbf{r}} + E_z\cos(\psi)\hat{\boldsymbol{\psi}}$, however, the ω^2 contribution from eq. (34) vanishes, thus not yielding such a shift.

If we now consider toroidal cholesterics rather than nematics, the chiral symmetry is broken explicitly (Fig. 4). A cholesteric pitch of $2\pi/q$ gives a contribution to the free energy of:

$$F_{cn} = K_2\,q\int \mathrm{d}V\;\; \mathbf{n}\cdot\nabla\times\mathbf{n}. \tag{35}$$

Substituting eq. 17 yields

$$\begin{aligned} F_{cn} &= -8\pi^2 K_2\,q\,R_1 R_2\,\xi\left(\xi - \sqrt{\xi^2-1}\right)\omega + \mathcal{O}\left(\omega^3\right) \\ &\approx -4\pi^2 K_2\,q\,R_1 R_2\,\omega + \mathcal{O}\left(\omega^3\right) \qquad \text{if } \xi \gg 1. \end{aligned} \tag{36}$$

Therefore, at the critical line in the phase diagram spanned by k and ξ, the degree of twist or surface angle scales (for large ξ) with the helicity of the cholesteric as

$$\alpha_{eq} \approx \left(2K_2R_2\,q/K_3\right)^{1/3} \sim q^{1/3}. \tag{37}$$

This is the analog scaling relation of $m_{eq} \sim H^{1/3}$ in the mean-field Ising model.

3.3 Results for the two-parameter Ansatz

Motivated by experiments[26], we can introduce an extra variational paramer γ to allow for splay deformations, in addition to ω:

$$n_\psi = \omega \frac{\xi r/R_2}{\xi + \gamma \frac{r}{R_2} \cos\psi}. \quad (38)$$

(Note that eqn 17 is recovered by setting $\gamma = 1$ in eqn 38.) In subsection 3.1 analytical results for $\gamma = 1$ were presented. In this subsection we will slightly improve these results by finding the optimal value of γ numerically. First, we discretise the azimuthally symmetric director field in the r and ψ direction. Next, we compute the Frank free energy density (eq. 1) by taking finite differences[43] of the discretised nematic field. After summation over the volume elements the Frank free energy will become a function of ω and γ for a given set of elastic constants and a given aspect ratio. Because of the normalisation condition on $\mathbf{n}$, the allowed values for ω and γ are constrained to the open diamond-like interval for which $-\xi < \gamma < \xi$ and $\frac{|\gamma|-\xi}{\xi} < \omega < \frac{\xi-|\gamma|}{\xi}$ holds.

The minima of the energy surface can be found by employing the conjugate gradient method. We have looked at the difference between the $\gamma = 1$ case and the case where the value of γ is chosen to minimise the energy. This was done for various choices of k. We have chosen the material properties of 5CB, *i.e.* $K_1 = 0.64K_3$ and $K_2 = 0.3K_3$[40]. The value for of K_{24} has not been so accurately determined, but previous measurements[26,44–48] seem to suggest that $K_{24} \approx K_2$, corresponding to $k \approx 0$.

We are interested in how the phase boundary changes by introducing the variational parameter γ. Therefore, the twist angle α, evaluated at the surface of the torus at $\psi = \frac{\pi}{2}$, versus the slenderness ξ is shown in the top panel of Fig. 6. For the particular choices of k there are two noticeable differences between the single-parameter Ansatz and the two-parameter Ansatz. Firstly, for small values of ξ, α is changed significantly. Secondly, for larger values of ξ we see that if there is a chiral-achiral phase transition, ξ_c is shifted by a small amount. In the bottom panel of Fig. 6 we further investigate how introducing γ influences the phase boundary, by plotting the phase boundary as a function of the toroidal slenderness ξ and elastic anisotropy k for both γ as a variational parameter (solid) and for $\gamma = 1$ (dashed). Observe that, for both the small ξ and small k regime, the difference is significant.

4 Conclusions

We have investigated spontaneous chiral symmetry breaking in toroidal nematic liquid crystals. As in the case of nematic tactoids[49,50], the two ingredients for this macroscopic chirality are orientational order of achiral microscopic constituents and a curved confining boundary. This phenomenon occurs when both the aspect ratio of the toroid and $\frac{K_2-K_{24}}{K_3}$ are small. The critical behavior of this structural transition belongs to the same universality class as the ferromagnet-paramagnet phase transition in the Ising model in dimensions above the upper critical dimension. The analogues of the magnetisation, reduced temperature and external field are the degree of twist (or surface angle), slenderness or $\frac{K_2-K_{24}}{K_3}$, and (cholesteric) helicity in liquid crystal toroids, respectively. Critical exponents are collected in Table 1.

Thus, the helicity rather than an external field breaks the chiral symmetry explicitly. Remarkably, since an external field couples quadratically to the director field, it induces a shift of the phase boundary. An azimuthally aligned field favours the mirror symmetric director configuration, whereas a homogeneous field in the z-direction favours the doubly twisted configuration.

A minimization of the elastic energy analogous to the one presented in this article for toroidal droplets, has also been carried out for spherical droplets[51]. The analytical results reproduce qualitatively the twisted textures observed experimentally in spherical bipolar droplets[52]. In this case, detailed measurements of the dependence of the twist angle on the elastic moduli were carried out by changing temperature which in turn affects the elastic moduli. The measured exponent β was 0.75 ± 0.1 for 8 CB and 0.76 ± 0.1 for 8 OCB[53], rather than the $\frac{1}{2}$ exponent we calculated in our mean field energy minimizations that entirely neglect thermal fluctuations.

Table 1 Dictionary of the critical behavior of the structural transition in liquid crystal toroids and the thermal phase transition in the mean-field Ising model.

Liquid crystal toroid	Mean-field Ising model	Exponent
$\alpha_{eq} \sim (-\delta\xi)^\beta$ $\alpha_{eq} \sim (-\delta k)^\beta$	$m_{eq} \sim (-t)^\beta$	$\beta = 1/2$
$\alpha_{eq} \sim q^{1/\delta}$	$m_{eq} \sim H^{1/\delta}$	$\delta = 3$

Acknowledgement

V.K. acknowledges funding from Stichting Fundamenteel Onderzoek der Materie (FOM). This work was partially supported by NSF DMR12-62047 and a Simons Investigator award from the Simons Foundation to RDK. We would like to thank Hiroshi Yokoyama for discussions.

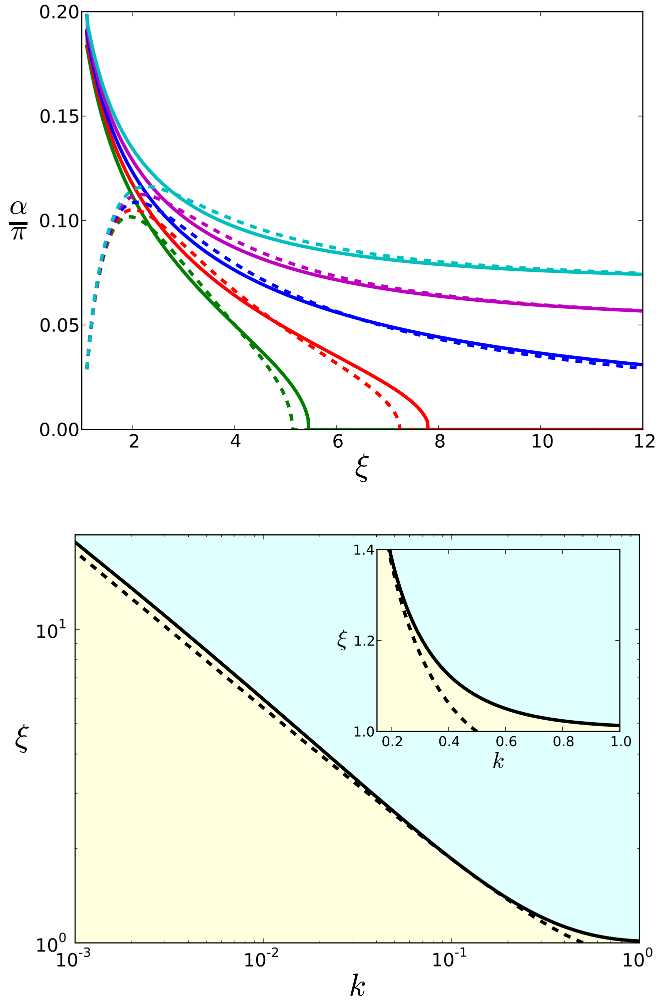

Fig. 6 *Top panel*: Twist angle α (in units of π) at $\psi = \pi/2$ versus the slenderness ξ for $k = 0.012$ (green), $k = 0.006$ (red), $k = 0$ (blue), $k = -0.006$ (magenta) and $k = -0.012$ (cyan). The dashed lines represent α for $\gamma = 1$, the solid lines represent α found for the optimal γ. *Bottom panel*: The phase boundary as a function of the toroidal slenderness ξ and elastic anisotropy k for γ as a variational parameter(solid) and for $\gamma = 1$ (dashed). The inset zooms in on the phase boundary for small ξ.

References

1 P. S. Drzaic, *Liquid crystal dispersions*, World Scientific, 1995.
2 O. D. Lavrentovich, *Liquid Crystals*, 1998, **24**, 117–126.
3 P. Poulin, *Current Opinion in Colloid & Interface Science*, 1999, **4**, 66 – 71.
4 H. Stark, *Physics Reports*, 2001, **351**, 387 – 474.
5 T. Lopez-Leon and A. Fernandez-Nieves, *Colloid and Polymer Science*, 2011, **289**, 345–359.
6 P. Poulin, H. Stark, T. C. Lubensky and D. A. Weitz, *Science*, 1997, **275**, 1770–1773.
7 T. C. Lubensky, D. Pettey, N. Currier and H. Stark, *Phys. Rev. E*, 1998, **57**, 610–625.
8 P. Poulin and D. A. Weitz, *Phys. Rev. E*, 1998, **57**, 626–637.
9 T. Araki and H. Tanaka, *Phys. Rev. Lett.*, 2006, **97**, 127801.
10 M. Ravnik, M. Škarabot, S. Žumer, U. Tkalec, I. Poberaj, D. Babič, N. Osterman and I. Muševič, *Phys. Rev. Lett.*, 2007, **99**, 247801.
11 U. Tkalec, M. Ravnik, S. Čopar, S. Žumer and I. Muševič, *Science*, 2011, **333**, 62–65.
12 V. S. R. Jampani, M. Škarabot, M. Ravnik, S. Čopar, S. Žumer and I. Muševič, *Phys. Rev. E*, 2011, **84**, 031703.
13 T. Lopez-Leon, V. Koning, K. B. S. Devaiah, V. Vitelli and A. Fernandez-Nieves, *Nature Physics*, 2011, **7**, 391–394.
14 V. Koning, T. Lopez-Leon, A. Fernandez-Nieves and V. Vitelli, *Soft Matter*, 2013, **9**, 4993–5003.
15 B. Senyuk, Q. Liu, S. He, R. D. Kamien, R. B. Kusner, T. C. Lubensky and I. I. Smalyukh, *Nature*, 2013, **493**, 200–205.
16 Q. Liu, B. Senyuk, M. Tasinkevych and I. I. Smalyukh, *Proceedings of the National Academy of Sciences*, 2013, **110**, 9231–9236.
17 M. Cavallaro Jr, M. A. Gharbi, D. A. Beller, S. Copar, Z. Shi, R. D. Kamien, S. Yang, T. Baumgart and K. J. Stebe, *Soft Matter*, 2013, **9**, 9099–9102.
18 J. Stelzer and R. Bernhard, *arXiv:cond-mat/0012394*, 2000.
19 M. Bowick, D. R. Nelson and A. Travesset, *Phys. Rev. E*, 2004, **69**, 041102.
20 I. M. Kulić, D. Andrienko and M. Deserno, *EPL (Europhysics Letters)*, 2004, **67**, 418.
21 L. Giomi and M. J. Bowick, *Phys. Rev. E*, 2008, **78**, 010601.
22 L. Giomi and M. J. Bowick, *Eur. Phys. J. E*, 2008, **27**, 275–296.
23 M. Bowick and L. Giomi, *Advances in Physics*, 2009, **58**, 449–563.
24 Z. Yao and M. O. de la Cruz, *Phys. Rev. E*, 2013, **87**, 012603.
25 R. L. B. Selinger, A. Konya, A. Travesset and J. V. Selinger, *The Journal of Physical Chemistry B*, 2011, **115**, 13989–13993.
26 E. Pairam, J. Vallamkondu, V. Koning, B. C. van Zuiden, P. W. Ellis, M. A. Bates, V. Vitelli and A. Fernandez-Nieves, *Proceedings of the National Academy of Sciences*, 2013, **110**, 9295–9300.
27 I. I. Smalyukh, Y. Lansac, N. A. Clark and R. P. Trivedi, *Nat Mater*, 2010, **9**, 139–145.
28 V. A. Bloomfield, *Biopolymers*, 1997, **44**, 269–282.
29 D. Marenduzzo, C. Micheletti, E. Orlandini and D. W. Sumners, *Proceedings of the National Academy of Sciences*, 2013, **110**, 20081–20086.
30 A. Leforestier and F. Livolant, *Proceedings of the National Academy of Sciences*, 2009, **106**, 9157–9162.
31 D. Marenduzzo, E. Orlandini, A. Stasiak, D. W. Sumners, L. Tubiana and C. Micheletti, *Proceedings of the National Academy of Sciences*, 2009, **106**, 22269–22274.
32 H. Shin and G. M. Grason, *EPL (Europhysics Letters)*, 2011, **96**, 36007.
33 Y. Hatwalne and M. Muthukumar, *Phys. Rev. Lett.*, 2010, **105**, 107801.
34 D. Svenšek and R. Podgornik, *EPL (Europhysics Letters)*, 2012, **100**, 66005.
35 I. M. Lifshitz, A. Y. Grosberg and A. R. Khokhlov, *Rev. Mod. Phys.*, 1978, **50**, 683–713.
36 M. Stevens, *Biophysical Journal*, 2001, **80**, 130–139.
37 M. R. Stukan, V. A. Ivanov, A. Y. Grosberg, W. Paul and K. Binder, *J. Chem. Phys.*, 2003, **118**, 3392–3400.
38 C. C. Conwell, I. D. Vilfan and N. V. Hud, *Proceedings of the National Academy of Science*, 2003, **100**, 9296–9301.
39 P. G. de Gennes and J. Prost, *The Physics of Liquid Crystals*, Oxford University Press, New York, 1993.
40 M. Kleman and O. D. Lavrentovich, *Soft Matter Physics: An Introduction*, Springer-Verlag New York, Inc., 2003.
41 R. D. Kamien, *Rev. Mod. Phys.*, 2002, **74**, 953–971.
42 R. B. Meyer, *Phys. Rev. Lett.*, 1969, **22**, 918–921.
43 B. Fornberg, *Mathematics of Computation*, 1988, **51**, 699–706.
44 D. W. Allender, G. P. Crawford and J. W. Doane, *Phys. Rev. Lett.*, 1991, **67**, 1442–1445.

45 O. D. Lavrentovich and V. M. Pergamenshchik, *Phys. Rev. Lett.*, 1994, **73**, 979–982.

46 R. D. Polak, G. P. Crawford, B. C. Kostival, J. W. Doane and S. Žumer, *Phys. Rev. E*, 1994, **49**, R978–R981.

47 A. Sparavigna, O. D. Lavrentovich and A. Strigazzi, *Phys. Rev. E*, 1994, **49**, 1344–1352.

48 O. Lavrentovich and V. Pergamenshchik, *International Journal of Modern Physics B*, 1995, **09**, 2389–2437.

49 P. Prinsen and P. van der Schoot, *Journal of Physics: Condensed Matter*, 2004, **16**, 8835.

50 L. Tortora and O. D. Lavrentovich, *Proceedings of the National Academy of Sciences*, 2011, **108**, 5163–5168.

51 R. D. Williams, *Journal of Physics A: Mathematical and General*, 1986, **19**, 3211.

52 G. E. Volovik and O. D. Lavrentovich, *Sov. Phys. JETP*, 1983, **58**, 1159–1166.

53 O. Lavrentovich and V. Sergan, *Il Nuovo Cimento D*, 1990, **12**, 1219–1222.

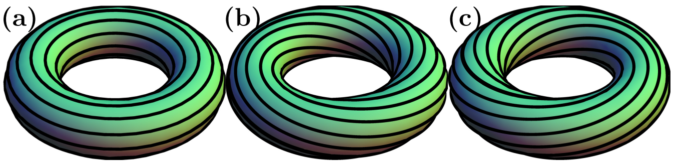

A structural transition between achiral (a) and chiral (b,c) nematic toroids occurs upon changing the slenderness or elastic constants.